FINITE ELEMENTS WITH AN EMBEDDED REINFORCEMENT FOR THE SIMULATION OF REINFORCED CONCRETE STRUCTURES STRENGTHENED WITH FRP

Francesco Riccardi*, Cédric Giry†, Fabrice Gatuingt‡

*,†,‡LMT, ENS Paris-Saclay, CNRS, Université Paris-Saclay
61 Avenue du Président Wilson, F-94235 Cachan, France
e-mail: {francesco.riccardi;cedric.giry;fabrice.gatuingt}@ens-paris-saclay.fr

Key words: FRP, Reinforced Concrete, Anchors, Interface

Abstract. The embedding of anchoring systems in the retrofitting of Reinforced Concrete (RC) structures by means of Fiber Reinforced Polymers (FRP) often implies local failure modes associated with high stress concentrations. In order to account for such mechanical behaviours in standard finite element computations, an explicit representation of interfaces is usually required. This strategy presents, however, several limitations in terms of computational cost and mesh-related issues. Specific finite elements for the simulation of pull-out mechanisms are here presented. The presence of interfaces is taken into account by enriching the displacement approximation by means of additional unknowns defined at the element level. Static-condensation, therefore, allows preserving the structure of the finite element procedure and limiting the computational effort.

1 INTRODUCTION

The good performances of FRP materials in enhancing the bearing capacity of RC structures have been well-acknowledged by extensive experimental campaigns during the last decades [1–5]. One of the main issues related to this technology is, however, the stress transfer between concrete and reinforcements, in particular under flexural loading conditions. Suitable anchoring systems are therefore required [6–9]. These often consist in composite strands which are glued through drilled holes to concrete. The latter are highly recommended especially in case of joints between vertical and horizontal elements, where non-anchored FRP strips fail in ensuring the load transfer, as pointed out in [10, 11]. The introduction of anchors mobilizes the tensile resistance of the reinforcement with shear stresses developing at the interface between FRP and concrete. The overall failure is then connected in most cases with the

anchor pull-out or its rupture, where debonding is often due to cracking of nearby concrete [9–11]. The choice of an appropriate numerical model for simulating the bending behaviour of RC structures strenghtened with FRP must then take into account the aforementioned observations. In mesoscale simulations, the discretization of the material boundaries allows achiving an explicit interface representation [12]. A more macroscopic approach adressed to large scale simulations consists in introducing kinematic relations between non-coincident DOFs, where bond-slip behaviours between concrete and reinforcements can be included by means of interface finite elements [13, 14]. A different strategy is to enrich the finite element approximation without resorting to remeshing techniques, by considering a similar framework as the Extended Finite Element Method (X-FEM) [15–17] and the Embedded Finite Element Method (E-FEM) [18–20]. In this paper, a
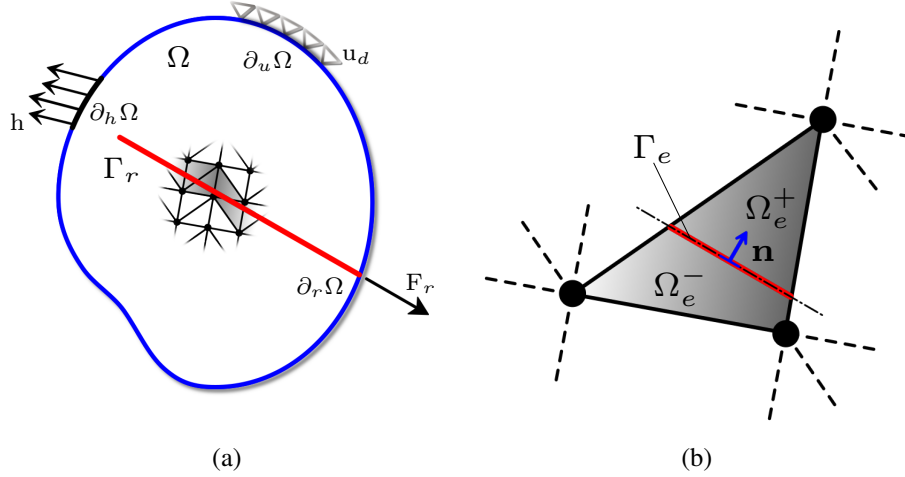
Figure 1: 2D body with an embedded anchor.

finite element model with enhanced kinematics for the simulation of structures with embedded anchors is presented. An enrichment is added to the macroscopic model in order to catch the interfacial behaviour associated with local shear stresses. The proposed formulation is validated at the element level for different configurations and compared to standard finite element simulations.

2 NUMERICAL MODEL

2.1 Spatial discretization

Let us consider a 2D body Ω and its boundary $\partial\Omega$, crossed by a reinforcement r whose axis is denoted by Γ_r (see Figure 1a). Dirichlet and Neumann boundary conditions are imposed on portions $\partial_u\Omega \subset \partial\Omega$ and $\partial_t\Omega \subset \partial\Omega$, respectively, such that $\partial\Omega = \partial_u\Omega \cup \partial_t\Omega$ and $\partial_u\Omega \cap \partial_t\Omega = \emptyset$. We also assume that there exists a part of the boundary $\partial_r\Omega \subset \partial_t\Omega$ where the resultant $\mathbf{F}_r$ acts. We indicate then with Ω_h the spatial discretization of Ω into N_e finite elements and $\Omega_h^r = \bigcup_{e=1}^{N_e^r} \Omega_e$ the set of elements crossed by Γ_r.

2.2 Finite element approximation

Each elementary domain $\Omega_e \in \Omega_h^r$, characterized by N nodes, is then decomposed into two subdomains Ω_e^+ and Ω_e^- as shown in Figure 1b. Its kinematics is approximated as follows:

$$\mathbf{u} \approx \mathbf{u}_h = \mathbf{N}\mathbf{d} + \mathbf{N}_r\mathbf{d}_r \qquad (1)$$

where $\mathbf{d}$ are the nodal displacements, $\mathbf{d}_r$ the enriching variables defined at the center of gravity of segment Γ_e, $\mathbf{N}$ is the standard shape function matrix and $\mathbf{N}_r$ is defined as:

$$\mathbf{N}_r = \begin{bmatrix} N_r & 0 \\ 0 & N_r \end{bmatrix} \qquad (2)$$

Function N_r is chosen such that the kinematic boundary conditions can still be expressed in terms of the sole nodal displacements, i.e. by imposing:

$$N_r\left(\mathbf{x}_j\right) = \mathbf{0} \quad , \quad \forall \mathbf{x}_j \in \Omega_h^r \qquad (3)$$

where $\mathbf{x}_j$ denotes the coordinates of node j. In addition, the compatible strain field reads:

$$\boldsymbol{\epsilon} \approx \boldsymbol{\epsilon}_h = \mathbf{B}\mathbf{d} + \mathbf{G}_r\mathbf{d}_r \qquad (4)$$

where $\mathbf{B} = \mathbf{L}\mathbf{N}$ and $\mathbf{G}_r = \mathbf{L}\mathbf{N}_r$ are the contributions to the strain field associated with the nodal and enhanced displacements ($\mathbf{L}$ computes ∇^s), respectively.

2.3 Governing equations

Let us consider the case of a single finite element. In absence of body forces, by applying the Principle of Virtual Works (PVW) and following a similar reasoning as for the SKON formulation proposed in the framework of the Embedded Finite Element Method (E-FEM) [19],

2
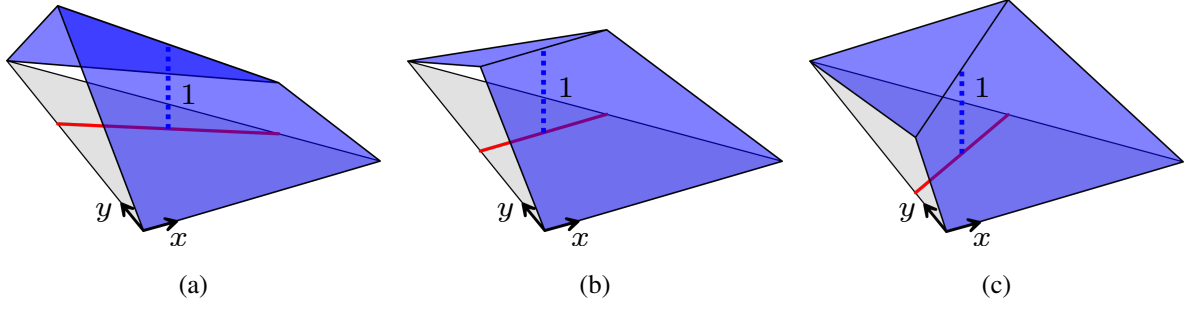
Figure 2: Function N_r in case of CST triangles for different anchor inclinations: (a) $\alpha_r = -20°$, (b) $\alpha_r = 0°$, (c) $\alpha_r = 20°$.

the governing equations reads:

$$\begin{cases} \displaystyle\int_{\Omega_e} \mathbf{B}^\mathsf{T}\boldsymbol{\sigma}\left(\boldsymbol{\epsilon}\right)\,\mathrm{d}A = \mathbf{F}^e_{ext} & (5a) \\[2mm] \displaystyle\int_{\Omega_e} \mathbf{G}^*_r\boldsymbol{\sigma}\left(\boldsymbol{\epsilon}\right)\,\mathrm{d}A = \mathbf{F}^e_r & (5b) \end{cases}$$

with

$$\mathbf{F}^e_{ext} = \int_{\partial_t\Omega_e} \mathbf{N}^\mathsf{T}\mathbf{h}\,\mathrm{d}\Gamma \qquad (6)$$

where $\boldsymbol{\sigma}\left(\boldsymbol{\epsilon}\right) = \boldsymbol{\sigma}\left(\mathbf{Bd} + \mathbf{G}_r\mathbf{d}_r\right)$ denotes the stress field and $\mathbf{G}^*_r$ is a matrix satisfying the condition of zero mean, defined as:

$$\mathbf{G}^*_r = \frac{1}{k_+ k_- l_{\Gamma_e}}\left(|\Omega^+_e|\chi_- - |\Omega^-_e|\chi_+\right)\mathbf{p}^\mathsf{T} \quad (7)$$

χ_+ and χ_-, denoting the characteristic functions of Ω^+_e and Ω^-_e, respectively; l_{Γ_e}, the length of segment Γ_e; $\mathbf{p}$, the matrix containing the components of the normal $\mathbf{n}$; k_+ and k_-, defined as:

$$k_+ = \frac{|\Omega^+_e|}{l_{\Gamma_e}} \quad , \quad k_- = \frac{|\Omega^-_e|}{l_{\Gamma_e}} \qquad (8)$$

Eq. (5a) states the global equilibrium between internal and external forces, whereas Eq. (5b) translates a local equilibrium condition along Γ_e.

2.4 Kinematic enrichment

After introducing the Heaviside function centered on Γ_e defined as:

$$\mathcal{H}_{\Gamma_e}(\mathbf{x}) = \begin{cases} 1, & \mathbf{x} \in \Omega^+_e \\ 0, & \mathbf{x} \in \Omega^-_e \end{cases} \qquad (9)$$

in the framework of a pull-out analysis, a possible choice for function N_r is:

$$\begin{aligned} N_r(\mathbf{x}) = &\chi_+ \sum_{i=1}^{N} a_i(1 - \mathcal{H}_{\Gamma_e}(\mathbf{x}_i))N_i(\mathbf{x}) \\ &+ \chi_- \sum_{i=1}^{N} a_i\mathcal{H}_{\Gamma_e}(\mathbf{x}_i)N_i(\mathbf{x}) \end{aligned} \qquad (10)$$

where N_i is the shape function associated with node i and constants a_i ensure a C^0- continuity across Γ_e (see Figure 2). $\mathbf{N}_r$ can be written in a compact form as:

$$\mathbf{N}_r = \chi_+\mathbf{N}(\mathbf{I} - \mathbf{H})\mathbf{A} + \chi_-\mathbf{N}\mathbf{H}\mathbf{A} \qquad (11)$$

where $\mathbf{I}$ and $\mathbf{H}$ are (2Nx2N) matrices and $\mathbf{A}$ is of dimension (2Nx2). Matrix $\mathbf{G}_r$ assumes then the following expression:

$$\mathbf{G}_r = \chi_+\mathbf{B}(\mathbf{I} - \mathbf{H})\mathbf{A} + \chi_-\mathbf{B}\mathbf{H}\mathbf{A} \qquad (12)$$

2.5 Resolution

In case of a linear elastic behaviour, the stress is expressed as:

$$\sigma = \mathbf{D}\boldsymbol{\epsilon} = \mathbf{D}\left(\mathbf{Bd} + \mathbf{G}_r\mathbf{d}_r\right) \qquad (13)$$

where $\mathbf{D}$ is the stiffness of the material. Substituting relation (13) into system (5), we obtain:

$$\begin{cases} \mathbf{K}^e_{bb}\mathbf{d} + \mathbf{K}^e_{bg}\mathbf{d}_r = \mathbf{F}^e_{ext} & (14a) \\ \mathbf{K}^e_{gb}\mathbf{d} + \mathbf{K}^e_{gg}\mathbf{d}_r = \mathbf{F}^e_r & (14b) \end{cases}$$

3
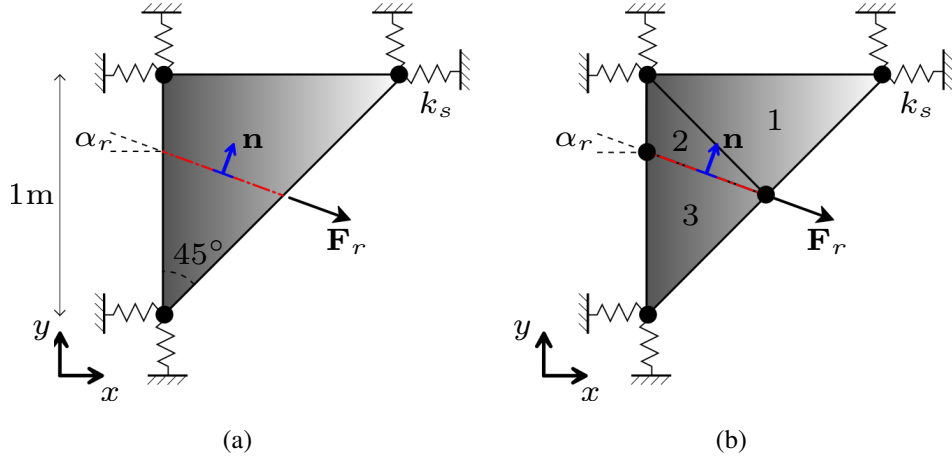
Figure 3: 2D case study: (1) macroscopic model, (2) mesoscopic model.

where we have defined the matrices:

$$\mathbf{K}_{bb}^e = \int_{\Omega_e} \mathbf{B}^\mathsf{T} \mathbf{D} \mathbf{B} \, \mathrm{d}A$$

$$\mathbf{K}_{bg}^e = \int_{\Omega_e} \mathbf{B}^\mathsf{T} \mathbf{D} \mathbf{G}_r \, \mathrm{d}A$$

$$\mathbf{K}_{gb}^e = \int_{\Omega_e} \mathbf{G}_r^* \mathbf{D} \mathbf{B} \, \mathrm{d}A \tag{15}$$

$$\mathbf{K}_{gg}^e = \int_{\Omega_e} \mathbf{G}_r^* \mathbf{D} \mathbf{G}_r \, \mathrm{d}A$$

If we collect $\mathbf{d}_r$ from equation (14b), we have:

$$\mathbf{d}_r = \left(\mathbf{K}_{gg}^e\right)^{-1} \left(\mathbf{F}_r^e - \mathbf{K}_{gb}^e \mathbf{d}\right) \tag{16}$$

The nodal displacements can therefore be computed by replacing expression (16) into equation (14a) as:

$$\mathbf{d} = \tilde{\mathbf{K}}_e^{-1} \left(\mathbf{F}_{ext}^e - \mathbf{K}_{bg}^e \left(\mathbf{K}_{gg}^e\right)^{-1} \mathbf{F}_r^e\right) \tag{17}$$

where

$$\tilde{\mathbf{K}}_e = \mathbf{K}_{bb}^e - \mathbf{K}_{bg}^e \left(\mathbf{K}_{gg}^e\right)^{-1} \mathbf{K}_{gb}^e \tag{18}$$

is the condensed stiffness matrix.

3 NUMERICAL VALIDATION

3.1 Problem description

Let us consider the case study depicted in Figure 3, where CST elements have been used. The effect of an embedded anchor is here represented by the force $\mathbf{F}_r = F_r \cos \alpha_r \mathbf{i}_x +$

$F_r \sin \alpha_r \mathbf{i}_y$, with $F_r = 10^5 \, \mathrm{N}$, applied in the middle of the right side of the structure. Linear springs with stiffness $k_s = 2.36 \times 10^9 \, \frac{\mathrm{N}}{\mathrm{m}}$ are introduced. The material parameters are $E = 30 \, \mathrm{GPa}$ and $\nu = 0.2$. Plane stress conditions are assumed for the computations (thickness $t = 0.1 \, \mathrm{m}$). The effect of the inclination α_r on the numerical response is studied while keeping the load application point fixed. The enhanced model presented in Section 2 is compared to standard finite elements. We will refer to "macroscopic" model in case of a single finite element and to "mesoscopic" model in case of an explicit interface, assumed as reference. The latter counts three finite elements and is decomposed into $\Omega^+ = \Omega_1 \cup \Omega_2$ and $\Omega^- \equiv \Omega_3$.

3.2 Results

The displacement u_F at the load application point, the local shear stress τ, computed as:

$$\tau = (\sigma_y - \sigma_x) \sin \alpha_r \cos \alpha_r + \tau_{xy} \left(\cos^2 \alpha_r - \sin^2 \alpha_r\right) \tag{19}$$

the principal stresses σ_I and σ_{II} and their directions α_I and α_{II} are compared. The total average $\bar{(\cdot)}$ of quantity $(\cdot)$ is computed as:

$$\bar{(\cdot)} = \frac{1}{|\Omega|} \int_\Omega (\cdot) \, \mathrm{d}A \tag{20}$$

4
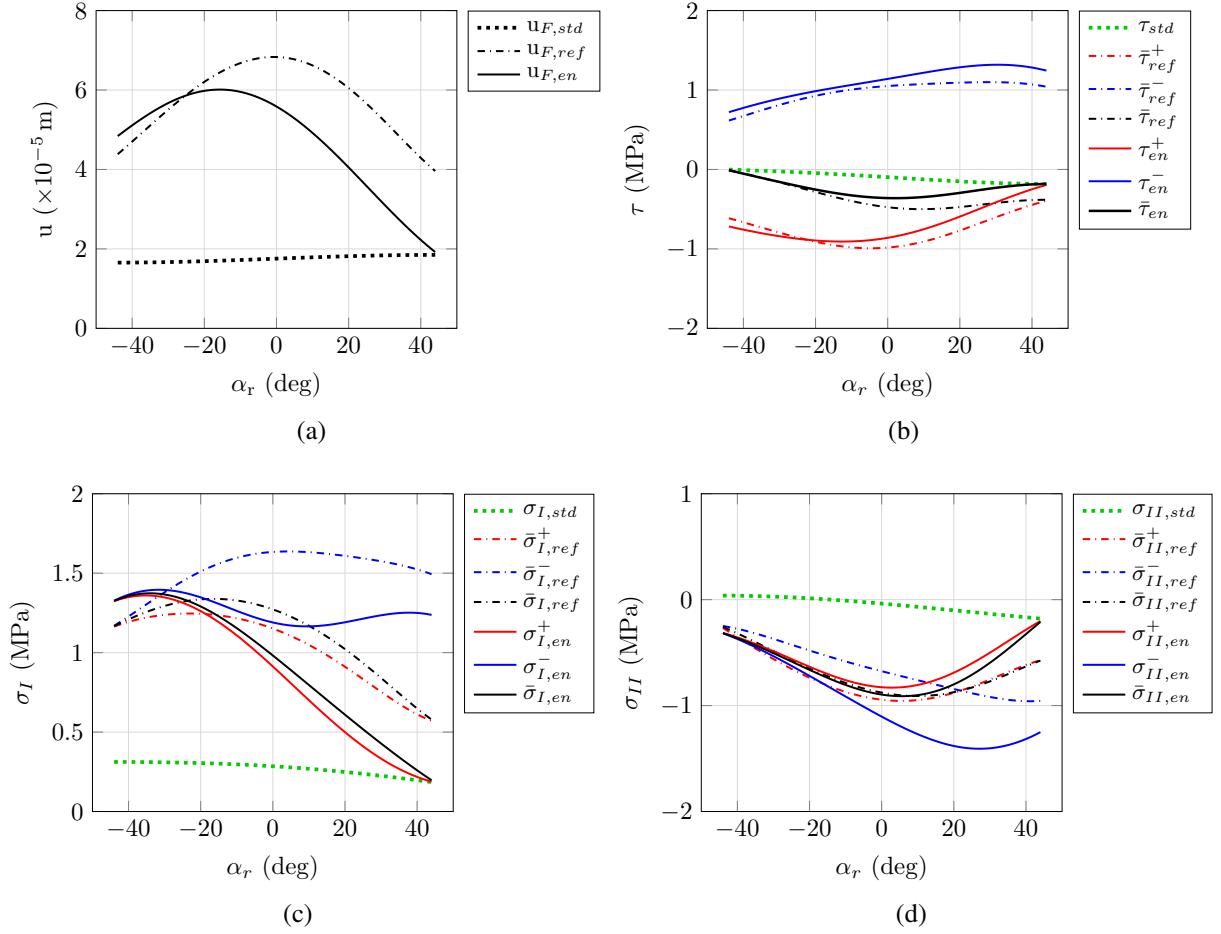
Figure 4: Comparative curves: displacement at load application point (a), shear stresses (b), maximum principal stresses (c), minimum principal stresses (d).

whereas local averages are defined as:

$$
\begin{aligned}
(\bar{\cdot})^{+} &= \frac{1}{|\Omega^{+}|} \int_{\Omega^{+}} (\cdot) \, \mathrm{d}A \\
(\bar{\cdot})^{-} &= \frac{1}{|\Omega^{-}|} \int_{\Omega^{-}} (\cdot) \, \mathrm{d}A
\end{aligned}
\tag{21}
$$

As can be seen in Figure 4, the enhanced macroscopic model performs pretty well with respect to the reference mesoscopic simulation, especially in computing local shear stresses (of opposite sign), whose total average value tends to zero as $|\Omega^{+}| = |\Omega^{-}|$ (when $\alpha_r \to -45°$, see Figure 4b). Such quantities govern the interfacial behaviour associated with pull-out mechanisms, which can not be reproduced by the standard macroscopic model. The evaluation of normal stresses is slightly less precise, but still satisfying (Figures 4c and 4d). As one can

see in Figure 5, the onset of a localized deformation mode does not affect significantly the overall average principal stress directions, i.e. $\bar{\alpha}_i \approx \bar{\alpha}_{i,ref} \approx \alpha_{i,std}$, $\forall \alpha_r$, with $i = I, II$. In Figure, 6 the resulting deformed shapes for $\alpha_r = -20°$ are shown, where the effect of the kinematic enhancement can be appreciated.

4 CONCLUSIONS

A finite element with enhanced kinematics for the simulation of structures with embedded anchors of arbitrary orientation has been proposed. An enrichment is added to the kinematic approximation for reproducing local mechanisms arising along the interface at the additional cost of solving a local equilibrium equation. The proposed model performs well with respect to a full model where the interface
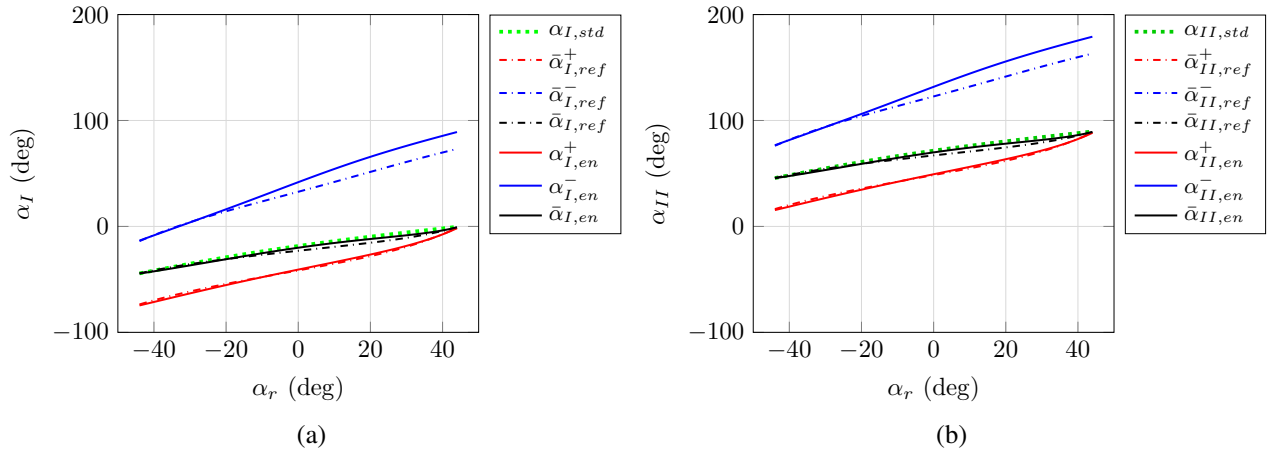
Figure 5: Comparative curves: maximum principal stress directions (a), minimum principal stress directions (b).

is explicity represented, especially in evaluating the shear stresses which are considered to be responsible for the experimentally observed debonding failure modes. Complete structural simulations, including nonlinear material responses, have to be performed in order to fully validate the proposed numerical model.

Acknowledgements

REFERENCES

[1] R Ma, Y Xiao and K Li. 2000. Full-scale testing of a parking structure column retrofitted with carbon fiber reinforced composites. *Construction and Building Materials*, 14(2):63–71.

[2] L De Lorenzis and A Nanni. 2001. Shear strengthening of reinforced concrete beams with near-surface mounted fiber-reinforced polymer rods. *Structural Journal*, 98(1):60–68.

[3] J A Barros, D R Ferreira, A S Fortes and S J Dias. 2006. Assessing the effectiveness of embedding CFRP laminates in the near surface for structural strengthening. *Construction and Building Materials*, 20(7):478–491.

[4] F Colomb, H Tobbi, E Ferrier and S P Hamelin. 2008. Seismic retrofit of reinforced concrete short columns by CFRP materials. *Composite Structures*, 82(4):475–487.

[5] S E El-Gamal, A Al-Nuaimi, A Al-Saidy and A Al-Lawati. 2016. Efficiency of near surface mounted technique using fiber reinforced polymers for the flexural strengthening of RC beams. *Construction and Building Materials*, 118:52–62.

[6] R Sadone, M Quiertant, S Chataigner, J Mercier and E Ferrier. 2011. Behavior of an innovative end-anchored externally bonded CFRP strengthening system under low cycle fatigue. In *Advances in FRP Composites in Civil Engineering*, 537–540. Springer, Berlin, Heidelberg.

[7] S T Smith, S Hu, S J Kim and R Seracino. 2011. FRP-strengthened RC slabs anchored with FRP anchors. *Engineering Structures*, 33(4):1075–1087.

[8] S Qazi, L Michel, and E Ferrier. 2013. Mechanical behaviour of slender RC walls
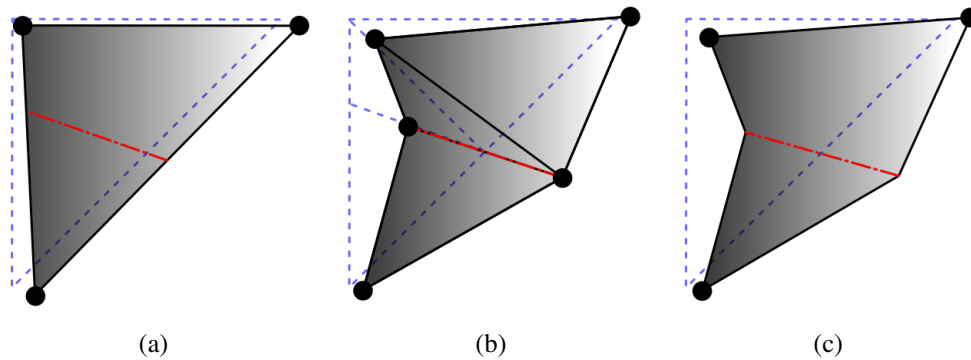
Figure 6: Amplified deformed shapes ($\alpha_r = -20°$): (a) standard macroscopic model, (b) mesoscopic model, (c) enhanced macroscopic model.

under seismic loading strengthened with externally bonded CFRP. *European Journal of Environmental and Civil Engineering*, 17(6):496–506.

[9] T Ozbakkaloglu and M Saatcioglu. 2009. Tensile behavior of FRP anchors in concrete. *Journal of Composites for Construction*, 13(2):453–461.

[10] F Ceroni, M Pecce, S Matthys and L Taerwe. 2008. Debonding strength and anchorage devices for reinforced concrete elements strengthened with FRP sheets. *Composites Part B: Engineering*, 39(3):429–441.

[11] S Qazi, L Michel and E Ferrier. 2013. Experimental investigation of CFRP anchorage systemsused for strengthening RC joints. *Composite Structures*, 99:453–461.

[12] V Palmieri and L De Lorenzis. 2014. Multiscale modeling of concrete and of the FRP–concrete interface. *Engineering Fracture Mechanics*, 131:150–175.

[13] A Casanova, L Jason, and L Davenne. 2012. Bond slip model for the simulation of reinforced concrete structures. *Engineering Structures*, 39:66–78.

[14] C Mang, L Jason, and L Davenne. 2015. A new bond slip model for reinforced concrete structures: Validation by modelling a reinforced concrete tie. *Engineering Computations*, 32(7):1934–1958.

[15] T Belytschko and T Black. 1999. Elastic crack growth in finite elements with minimal remeshing. *International journal for numerical methods in engineering*, 45(5):601–620.

[16] N Moës, J Dolbow and T Belytschko. 1999. A finite element method for crack growth without remeshing. *International Journal for Numerical Methods in Engineering*, 46(1):131–150.

[17] J Dolbow, N Moës and T Belytschko. 2000. Discontinuous enrichment in finite elements with a partition of unity method. *Finite Elements in Analysis and Design*, 36(3):235–260.

[18] F Armero and K Garikipati. 1996. An analysis of strong discontinuities in multiplicative finite strain plasticity and their relation with the numerical simulation of strain localization in solids. *International Journal of Solids and Structures*, 133(20):2863–85.

[19] M Jirásek. 2000. Comparative study on finite elements with embedded discontinuities. *Computer Methods in Applied Mechanics and Engineering*, 188(1):307–330.

[20] J Oliver, A E Huespe and P J Sánchez. 2000. A comparative study on finite elements for capturing strong discontinuities: E-FEM vs X-FEM. *Computer Methods in Applied Mechanics and Engineering*, 195(37–40):4732–4752.